THE JOURNAL OF PHYSICAL CHEMISTRY C
A JOURNAL OF THE AMERICAN CHEMICAL SOCIETY

pubs.acs.org/JPCC Article

Volatile Products from Ligand Addition of $P(CH_3)_3$ to $NiCl_2$, $PdCl_2$, and $PtCl_2$: Pathway for Metal Thermal Atomic Layer Etching

Published as part of The Journal of Physical Chemistry virtual special issue "Cynthia Friend Festschrift".

Ann Lii-Rosales, Virginia L. Johnson, Sandeep Sharma, Andreas Fischer, Thorsten Lill, and Steven M. George*

Cite This: *J. Phys. Chem. C* 2022, 126, 8287−8295 Read Online

ABSTRACT: $NiCl_2$, $PdCl_2$, and $PtCl_2$ can be spontaneously etched by ligand addition with $P(CH_3)_3$ ($P(Me)_3$, trimethylphosphine). Ligand addition of $P(Me)_3$ to these group 10 metal chlorides can form stable and volatile complexes. These ligand-addition reactions are suggested by the covalent bond classification (CBC) method. The CBC method provides guidelines for determining probable transition metal complexes based upon the stoichiometry of the metal (M), one-electron donor ligands (X), and electron-pair donor ligands (L). The CBC model predicts that a complex with a stoichiometry of MX_2L_2 is most frequently observed for Ni, Pd, and Pt. This prediction suggests that $MCl_2(P(Me)_3)_2$ is a likely stable product after exposing Ni, Pd, and Pt to chlorination and then ligand-addition reactions with $P(Me)_3$. In accordance with these expectations, *in situ* QMS studies revealed that $NiCl_2(P(Me)_3)_2^+$, $PdCl_2(P(Me)_3)_2^+$, and $PtCl_2(P(Me)_3)_2^+$ were observed as volatile metal complexes resulting from $P(Me)_3$ exposure to $NiCl_2$, $PdCl_2$, and $PtCl_2$. Thermochemical calculations also indicated that addition of $P(Me)_3$ to MCl_2 and $MCl_2(P(Me)_3)$ was favorable where M = Ni, Pd, and Pt. The identification of these volatile products and the theoretical verification of their stability suggest that pathways for Ni, Pd, and Pt thermal atomic layer etching (ALE) are possible based on sequential chlorination and ligand-exchange reactions.

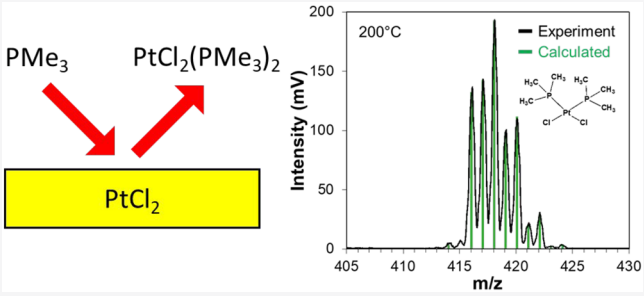

1. INTRODUCTION

Dry etching plays an important role in semiconductor processing to fabricate three-dimensional structures.[1] This dry etching is usually performed using reactive species from plasmas.[2] Ionic species from plasmas are particularly important because they can provide the anisotropy needed for directional etching.[3] The use of plasmas for etching is so common that the prevailing view is that dry etching usually requires a plasma. However, there are also many examples of dry etching based on spontaneous thermal etching. The most familiar examples involve silicon etching by the formation of volatile fluorides after exposure to fluorination reactants such as XeF_2.[4,5] Other examples include the etching of metals such as tungsten, copper, and aluminum by halogenation reactants such as XeF_2 or Cl_2.[6−8]

Spontaneous thermal etching is also important in thermal atomic layer etching (ALE) processes.[9,10] Thermal ALE is defined by sequential surface modification and volatile release reactions that remove material with atomic layer control.[9,10] To obtain atomic layer control, at least one of the reactions must be self-limiting.[11,12] For the known thermal ALE processes, the surface modification reaction is the self-limiting reaction.[13] The volatile release reaction in thermal ALE can be non-self-limiting, i.e., continuous or spontaneous, if the surface modification reaction is self-limiting.[11−13] Many thermal ALE reactions have been developed recently for a variety of materials.[9] Thermal ALE has been defined for metal oxides including Al_2O_3,[14−16] HfO_2,[17,18] ZnO,[19] and Ga_2O_3.[20] Procedures for thermal ALE have been described for metal nitrides such as AlN,[21] TiN,[22] and GaN.[23] Thermal ALE has been established for silicon-based materials including Si,[24] SiO_2,[25] Si_3N_4,[26] and SiGe.[27] In addition, thermal ALE has been developed for metals such as W,[28] Cu,[29] and Co.[30]

One of the main mechanisms for these thermal ALE processes is based on fluorination for surface modification and ligand exchange for volatile release.[10,16,31] The fluorination reaction is often performed using HF.[10,14,16] Ligand exchange is a transmetalation reaction where a ligand from the incoming

Received: December 19, 2021
Revised: April 21, 2022
Published: May 9, 2022

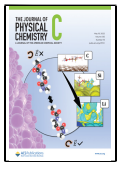

https://doi.org/10.1021/acs.jpcc.1c10690
J. Phys. Chem. C 2022, 126, 8287−8295

precursor is transferred to the metal fluoride and a fluoride ligand from the metal fluoride is transferred to the incoming precursor.[10,31−33] The ligand-exchange mechanism leads to a ligand substitution. Prominent ligands from ligand-exchange precursors undergoing ligand exchange, such as $Al(CH_3)_3$ and $TiCl_4$, have been CH_3 and Cl, respectively.[15,17] The reaction between the ligand-exchange precursor and the metal fluoride has been observed to be a spontaneous reaction.[34,35]

Other volatile release mechanisms for thermal ALE may exist in addition to ligand exchange. One important mechanism that has not been explored thoroughly for thermal ALE is ligand addition. The ligand-addition mechanism involves adding a new ligand to an existing complex to enable the volatilization of the complex. Ligand-addition processes such as oxidative addition are well-known in organometallic solution chemistry.[36] However, few reports exist for ligand addition leading to a volatile complex. One example is the ligand addition of pyridine (py) to $CoCl_2$ to yield the volatile $CoCl_2py_2$ complex.[37,38] The $CoCl_2py_2$ complex has been studied in the gas phase using UV−visible absorption spectroscopy.[37] Another example is the ligand addition of $P(CH_2CH_3)_3$ to CuCl to yield the volatile $CuCl(P(CH_2CH_3)_3)_2$ complex.[39−41] The $CuCl(P(CH_2CH_3)_3)_2$ complex has been identified by mass spectrometry studies.[39,40]

Other examples related to ligand addition involve the addition of acetylacetone (Hacac) or hexafluoroacetylacetone (Hhfac) to metal oxides to yield volatile metal acetylacetone complexes.[29,42] In this case, hydrogen from the Hacac or Hhfac is believed to combine with oxygen from the metal oxide to form H_2O.[29] Hacac or Hhfac can also be exposed to metal chlorides to yield volatile metal acetylacetone complexes.[30,43] These reactions have been interpreted as substitution reactions where hydrogen from Hacac combines with chlorine to form HCl.[43] Attempts to observe volatile Cl-containing metal acetylacetone complexes have been inconclusive.[30]

Possible stable and potentially volatile metal complexes during metal thermal ALE are suggested by the covalent bond classification (CBC) method.[44] The CBC method reports the probable stable complexes for a given metal resulting from bonding to various ligands. The complexes can be expressed as MX_xL_y where M is the metal center, X is a one-electron donor ligand, and L is an electron-pair donor ligand.[44] To form a stable metal complex, X and L ligands are added to the metal center. Generally, the most stable complexes will satisfy the 16 or 18 electron rule.[36] The MLX plots report the probability for occurrence of the various MX_xL_y complexes based on metal species documented in the Dictionary of Organometallic Compounds.[45] The MLX plot for Ni is shown in Figure 1.[46] The MLX plots provide guidance to define the sequential surface reactions for metal thermal ALE.

This paper reports the volatile products from the spontaneous etching of $NiCl_2$, $PdCl_2$, and $PtCl_2$ by ligand addition with $P(Me)_3$. Metal chloride powders are used to represent chlorinated metal surfaces that would be present following chlorination of the elemental metal surface in a metal thermal ALE process defined by chlorination and ligand-addition reactions. $P(Me)_3$ is flowed through the metal chloride powder to determine if the metal chloride can be volatilized by ligand addition. The metal chloride powder provides a nearly infinite reservoir of metal chloride that supplies much more volatile etch product for the quadrupole mass spectrometry (QMS) studies.

Ni		Electron Number								
		12	13	14	15	16	17	18	19	20
Valence Number	0	ML <1%		ML_2 1%		ML_3 14%		ML_4 16%		ML_5 <1%
	1		MXL		MXL_2		MXL_3 <1%		MXL_4 <1%	
	2	MX_2 <1%		MX_2L <1%		MX_2L_2 33%		MX_2L_3 26%		MX_2L_4 3%
	3		MX_3		MX_3L		MX_3L_2 <1%		MX_3L_3 <1%	
	4	MX_2Z		MX_4		MX_4L <1%		MX_4L_2 4%		MX_4L_3 <1%

Figure 1. MLX plot of possible Ni complexes. M is metal center, X is one-electron donor ligand, and L is electron pair donor ligand. Percentages report probability of occurrence of metal complexes are based on the Dictionary of Organometallic Compounds.[45]

The stable volatile metal complexes identified by QMS are then compared with the expectations from the CBC method. The stability of these volatile metal products is also confirmed using quantum chemical calculations. We note that recent results have been reported for thermal Ni ALE defined by sequential chlorination and ligand-addition reactions where SO_2Cl_2 was the chlorine reactant and $P(Me)_3$ was the ligand-addition reactant.[47] In addition, recent QMS studies have monitored the volatile gas products from the ligand addition of $P(Me)_3$ to $NiCl_2$ powder.[47]

2. EXPERIMENTAL SECTION

2.A. QMS Detection of Volatile Etch Species. Detection of the volatile etch species produced during the ligand-addition reactions was accomplished using a quadrupole mass spectrometer (QMS; Extrel MAX-QMS flange mounted system). Details of the QMS and reactor setup have been reported elsewhere.[34] Metal chloride powders utilized in the QMS experiments included $NiCl_2$ (99.99+%, Strem Chemicals), $PdCl_2$ (99.9%, Strem Chemicals), and $PtCl_2$ (99.9%, Strem Chemicals). $P(Me)_3$ (trimethylphosphine, 97%, Sigma-Aldrich) was used as the precursor for ligand addition. $P(Me)_3$ is toxic and pyrophoric. $P(Me)_3$ should not be exposed to air or moisture. Precautions should be taken when handling $P(Me)_3$. For example, $P(Me)_3$ was transferred in a glovebox under inert atmosphere to protect the operator and the chemical integrity of the $P(Me)_3$.

During the experiments, a N_2 carrier gas flowed through the metal chloride powders at a pressure of ≈1.8 Torr. In addition, the partial pressure of $P(Me)_3$ flowing through the metal chloride powders was ≈0.5 Torr. For the temperature ramp studies, a linear heating rate of 3 °C/min was used to survey the volatile products. During the temperature ramp, the pressures of the $P(Me)_3$ and N_2 carrier gas were constant. They were continuously flowed through the metal chloride powders unless stated otherwise.

All volatile species were entrained in a molecular beam. Details about the molecular beam generation in this reactor have been reported elsewhere.[34] This molecular beam exited the sample holder, traveled through a differentially pumped volume, passed through a skimmer, and then entered a differentially pumped region around the ionizer of the mass spectrometer. The molecular beam was categorized as intermediate or partially hydrodynamic based on the Knudsen

https://doi.org/10.1021/acs.jpcc.1c10690
J. Phys. Chem. C 2022, 126, 8287−8295

number (Kn) of Kn = 0.05−0.08.[48] The molecular beam was positioned with line-of-sight to the QMS ionizer entrance for direct and accurate detection. The molecular beam increased the intensity of the volatile species.

Isotopic distributions of the volatile etch products were calculated based on the naturally occurring isotopic abundances of a compound. For example, for $PtCl_2(P(Me)_3)_2$, all five isotopes of Pt (^{192}Pt, ^{194}Pt, ^{195}Pt, ^{196}Pt, ^{198}Pt), all isotopes of Cl (^{35}Cl, ^{37}Cl), and all isotopes of P, C, and H were utilized to generate the expected isotopic patterns. The isotopes of Ni, Pd, and Pt are distinct and characteristic of the corresponding mass spectra of the etch products. The Cl isotopes are also distinguishing and help to identify the number of Cl atoms in the etch products.

2.B. Computational Details. Sequential additions of $P(Me)_3$ precursor to MCl_2 (M = Ni, Pd, Pt) were studied with a combination of *ab initio* and thermodynamic calculations. All quantum chemical calculations were performed using Gaussian 16.[49] The optimization of all geometries was completed at the UB3LYP/Def2TZVP level of theory.[50,51] These geometries were used to calculate single point energies with UCCSD(T)/sdd.[52−55]

Gibbs free energies were calculated using translational, vibrational, and rotational degrees of freedom at 100 °C along with UCCSD(T) energies. Harmonic vibrational frequencies were obtained from UB3LYP/Def2TZVP geometries. The thermochemical methods have been discussed in depth.[56] The RMACC Summit Supercomputer was used for all calculations.[57]

3. RESULTS AND DISCUSSION

3.A. Ligand Addition of $P(Me)_3$ to $NiCl_2$. Exposure of $P(Me)_3$ to $NiCl_2$ yielded $NiCl_2(P(Me)_3)_2^+$ as a volatile product. The QMS results at 92 °C are shown in Figure 2. The isotopic fingerprints are consistent with the presence of ^{58}Ni and ^{60}Ni isotopes, as well as ^{35}Cl and ^{37}Cl isotopes. The peak at m/z 280 agrees with $^{58}Ni^{35}Cl_2(P(Me)_3)_2^+$. The peak at m/z 282 can be attributed to $^{58}Ni^{35}Cl^{37}Cl(P(Me)_3)_2^+$ and/or $^{60}Ni^{35}Cl_2(P(Me)_3)_2^+$. The peak at m/z 284 is assigned to $^{58}Ni^{37}Cl_2(P(Me)_3)_2^+$ and/or $^{60}Ni^{35}Cl^{37}Cl(P(Me)_3)_2^+$. These peaks are consistent with the ligand-addition reaction of $P(Me)_3$ to the Ni metal center in $NiCl_2$.

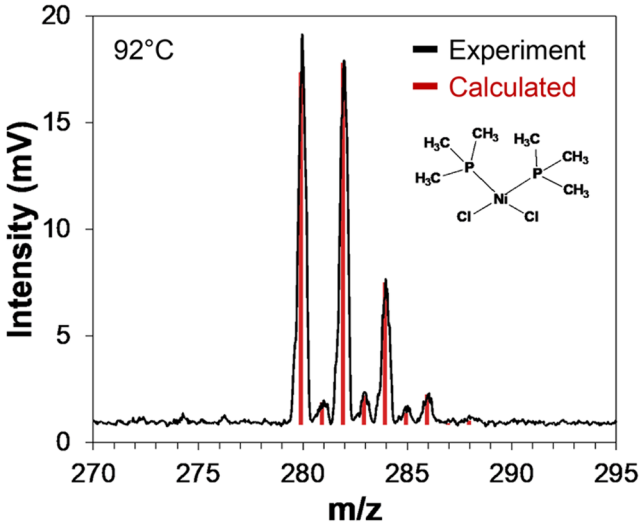

Figure 2. Mass spectrum of $NiCl_2(P(Me)_3)_2^+$ from $P(Me)_3$ exposure to $NiCl_2$ powder at 92 °C.

The $NiCl_2(P(Me)_3)_2^+$ product agrees with Ni organometallic complexes with a stoichiometry of MX_2L_2, where the X ligand (one electron donor) is Cl, and the L ligand (electron pair donor) is $P(Me)_3$. This product was expected based on the MLX plot for Ni from the CBC method shown in Figure 1.[46] The two Cl ligands and two $P(Me)_3$ ligands in $NiCl_2(P(Me)_3)_2$ satisfy the 16-electron rule where there are 16 electrons in the outer shell of Ni for stabilization.[44]

The intensity of the $NiCl_2(P(Me)_3)_2^+$ product as a function of the sample temperature is shown in Figure 3. The

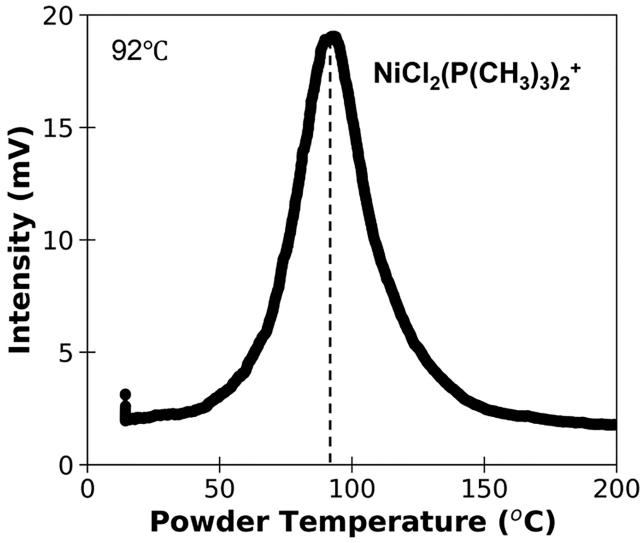

Figure 3. Ion intensity of $NiCl_2(P(Me)_3)_2^+$ as a function of powder temperature during $P(Me)_3$ exposure to $NiCl_2$ powder during a linear heating rate of 3 °C/min.

$NiCl_2(P(Me)_3)_2^+$ product has a peak intensity at 92 °C. There are onset product intensities as low as 65 °C. The product appearance may be either desorption or reaction limited. For desorption-limited product appearance, the product may form at lower temperatures but requires more thermal energy for desorption. For reaction-limited product appearance, the product may not desorb until the temperature where the product is formed on the surface.

Above 92 °C, the product intensity decreases with temperature. This decrease could result from the decreasing residence time of the $P(Me)_3$ precursor. This $P(Me)_3$ precursor may precede the formation of the volatile $NiCl_2(P(Me)_3)_2$ product. The decreasing intensity of $NiCl_2(P(Me)_3)_2$ at higher temperatures could be fit using a precursor-mediated adsorption model.[58] $NiCl_2(P(Me)_3)_2$ is stable at these temperatures. $NiCl_2(P(Me)_3)_2$ has been reported to have a melting point in the range of 194−199 °C.[59]

3.B. Cold or Hot Exposures of $P(Me)_3$ to $NiCl_2$. Additional experiments were performed to explore whether the appearance of the $NiCl_2(P(Me)_3)_2$ product was desorption-limited or reaction-limited. In these experiments, $P(Me)_3$ was exposed to the $NiCl_2$ powder either below or above the appearance of the $NiCl_2(P(Me)_3)_2$ product in Figure 3. Subsequently, the sample was either ramped up or ramped down in temperature in the presence of only N_2 carrier gas. The details of the cold and hot exposure experiments are illustrated in Figure 4.

https://doi.org/10.1021/acs.jpcc.1c10690
J. Phys. Chem. C 2022, 126, 8287−8295

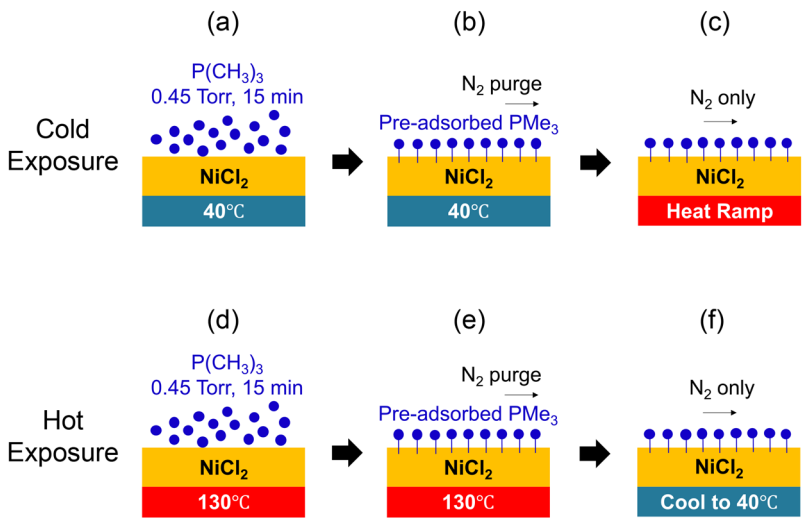

Figure 4. Cold exposure procedure: (a) $P(Me)_3$ exposure to $NiCl_2$ powder at 40 °C followed by (b) N_2 purging and (c) heat ramp during N_2 purging. Hot exposure procedure: (d) $P(Me)_3$ exposure to $NiCl_2$ powder at 130 °C followed by (e) N_2 purging and (f) cool down during N_2 purging.

Figure 4a−c shows schematics of the cold exposure experiment. The $NiCl_2$ sample was held around room temperature and exposed to 0.45 Torr of $P(Me)_3$ for 15 min (Figure 4a). No N_2 carrier gas was used during the cold exposure. After 15 min, the $P(Me)_3$ exposure was ended and the $NiCl_2$ sample was purged by N_2 to remove any residual $P(Me)_3$ inside the sample holder (Figure 4b). The purge was stopped when no more $P(Me)_3$ was observed by the QMS. Subsequently, the $NiCl_2$ sample was ramped up in temperature in the presence of only N_2 carrier gas (Figure 4c). No $P(Me)_3$ was exposed to the $NiCl_2$ powder during this temperature ramp.

The blue data points in Figure 5 show the results of the temperature ramp after the cold exposure. $NiCl_2(P(Me)_3)_2^+$ was observed with a peak intensity at approximately 82 °C. The appearance of $NiCl_2(P(Me)_3)_2^+$ indicates that this complex must have formed at room temperature. However, $NiCl_2(P(Me)_3)_2^+$ was not observed at room temperature during the temperature ramp experiment shown in Figure 3. The product volatilization must be thermally driven and only occurs at higher temperatures.

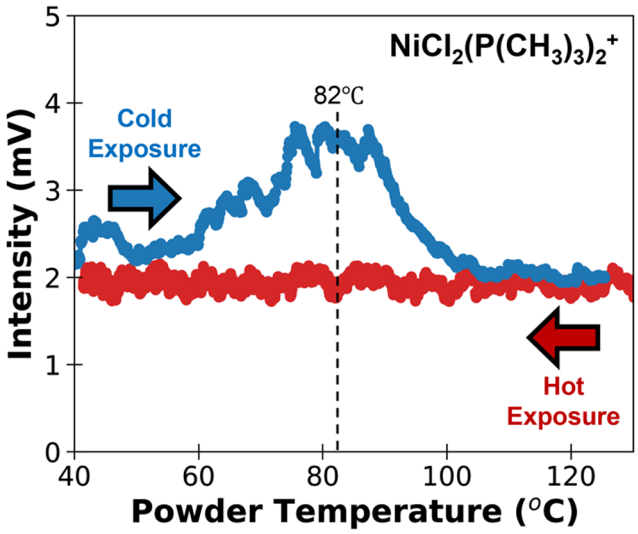

Figure 5. Ion intensity of $NiCl_2(P(Me)_3)_2^+$ as a function of $NiCl_2$ powder temperature during (a) cold exposure procedure (blue points) and (b) hot exposure procedure (red points).

There is also a large difference in signal intensities between the two linear temperature ramp experiments. The peak product intensity was ∼18 mV at 92 °C for the temperature ramp experiment conducted with continuous $P(Me)_3$ exposure shown in Figure 3. The product intensity was ∼3.5 mV at 82 °C for the linear temperature ramp experiment performed after the cold exposure followed by only N_2 carrier gas displayed in Figure 5. This difference in signal intensities indicates that much more volatile $NiCl_2(P(Me)_3)_2$ product can form at 92 °C at the peak intensity compared with the $NiCl_2(P(Me)_3)_2$ product that is stored on the $NiCl_2$ powder after $P(Me)_3$ exposures at room temperature and then desorbs with a peak intensity at 82 °C.

The results are very different for the hot exposure experiment. Figure 4d−f shows schematics of the hot exposure experiment. In these experiments, the $NiCl_2$ sample was held at 130 °C and exposed to 0.45 Torr of $P(Me)_3$ for 15 min (Figure 4d). No N_2 carrier gas was used during the hot exposure. After 15 min, the $P(Me)_3$ exposure was ended and the $NiCl_2$ sample was purged by N_2 to remove any residual $P(Me)_3$ inside the sample holder (Figure 4e). The purge was stopped when no more $P(Me)_3$ was observed by the QMS. Subsequently, the $NiCl_2$ sample was ramped down in temperature in the presence of only N_2 carrier gas (Figure 4f). No $P(Me)_3$ was exposed to the $NiCl_2$ powder during this cooling temperature ramp.

The results of the hot exposure experiment are shown by the red data points in Figure 5. With the $NiCl_2$ powder held at 130 °C, the $P(Me)_3$ exposure did not lead to the formation of $NiCl_2(P(Me)_3)_2$. These results are in agreement with the results in Figure 3. The lack of $NiCl_2(P(Me)_3)_2$ formation at 130 °C suggests that the residence time of $P(Me)_3$ is too short to add to $NiCl_2$ and form $NiCl_2(P(Me)_3)_2$. In addition, the subsequent temperature ramp from 130 °C down to 40 °C in the absence of $P(Me)_3$ exposure also did also not yield any $NiCl_2(P(Me)_3)_2$ product as shown in Figure 5.

https://doi.org/10.1021/acs.jpcc.1c10690
J. Phys. Chem. C 2022, 126, 8287−8295

3.C. Ligand Addition of $P(Me)_3$ to $PdCl_2$. The strategy of ligand addition can be extended to other group 10 metal chlorides. On the basis of the MLX plot for Pd from the CBC method, MX_2L_2 is a stable complex with a probability of occurrence of 81%.[46] MX_2L_2 has the same stoichiometry as the Ni complex, $NiCl_2(P(Me)_3)_2$, described above. In similarity with the Ni MX_2L_2 complex, this Pd MX_2L_2 complex also obeys the 16-electron rule.

An equivalent approach to the methods employed for $NiCl_2$ was utilized to study the spontaneous etching of $PdCl_2$ using $P(Me)_3$ for the ligand-addition reaction. The results for these experiments at 150 °C are shown in Figure 6. The QMS analysis observed a cluster of ion intensities with the highest intensity peak at m/z 330. On the basis of the distribution of isotopic fingerprints, this cluster is assigned to $PdCl_2(P(Me)_3)_2^+$. The experimental ion intensities and the calculated ion intensities based on the isotopic abundances are in excellent agreement as shown in Figure 6. This $PdCl_2(P(Me)_3)_2^+$ ion is the parent of the MX_2L_2 complex that was expected from the Pd MLX plot.

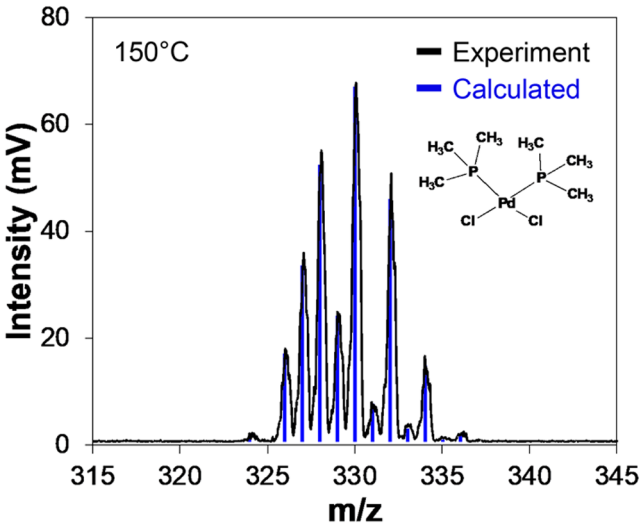

Figure 6. Mass spectrum of $PdCl_2(P(Me)_3)_2^+$ from $P(Me)_3$ exposure to $PdCl_2$ powder at 150 °C.

The intensity of the $PdCl_2(P(Me)_3)_2^+$ product as a function of the sample temperature is shown in Figure 7. For this linear temperature ramp experiment, the $PdCl_2(P(Me)_3)_2^+$ signals have an onset at 85 °C. The peak ion intensity is observed at 150 °C. Ion intensities are also observed at temperatures as high as 275 °C. The temperature ramp results for $NiCl_2$ in Figure 3 and $PdCl_2$ in Figure 7 are different. These temperature differences could reflect variations in the (i) vapor pressures of the complexes, (ii) residence times of $P(Me)_3$ on the surface ($PdCl_2$ versus $NiCl_2$), or (iii) overall reaction kinetics. The vapor pressure of $PdCl_2(P(Me)_3)_2$ is not reported in the literature to the best of our knowledge.

3.D. Ligand Addition of $P(Me)_3$ to $PtCl_2$. The spontaneous etching of $NiCl_2$ and $PdCl_2$ reported above suggests that $PtCl_2$ may also be spontaneously etched by ligand addition with $P(Me)_3$. The spontaneous etching of $PtCl_2$ was explored using QMS analysis with the same experimental conditions as for the spontaneous etching of $NiCl_2$ and $PdCl_2$. The CBC method can also be used to predict the probable release of volatile Pt complexes. On the basis of the MLX plot for Pt from the CBC method, MX_2L_2 is a stable complex with a probability of occurrence of 69%.[46] This Pt MX_2L_2 complex has the same stoichiometry as the Ni and Pd complexes described above. This Pt MX_2L_2 complex also obeys the 16-electron rule.

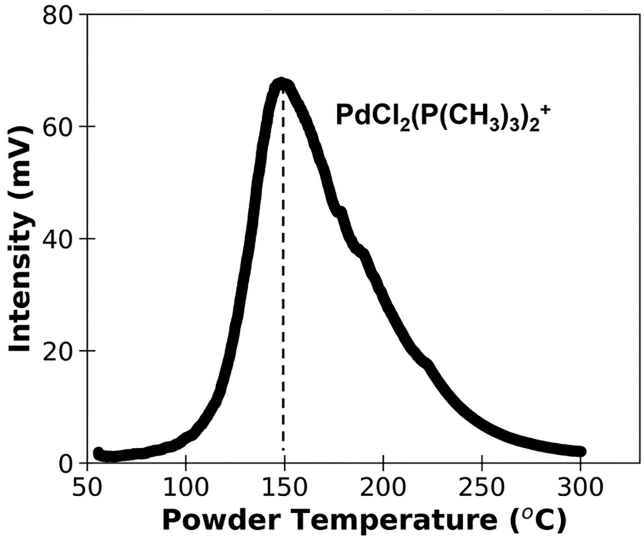

Figure 7. Ion intensity of $PdCl_2(P(Me)_3)_2^+$ as a function of powder temperature during $P(Me)_3$ exposure to $PdCl_2$ powder.

By exposure of $P(Me)_3$ to $PtCl_2$, $PtCl_2(P(Me)_3)_2^+$ was observed by QMS analysis as shown in Figure 8. This $PtCl_2(P(Me)_3)_2^+$ ion signal has a characteristic signature that reflects the natural abundances of the Pt and Cl isotopes. The experimental ion intensities and the calculated ion intensities based on the isotopic abundances are in excellent agreement as shown in Figure 8. This $PtCl_2(P(Me)_3)_2^+$ ion is the parent of the MX_2L_2 complex that was expected from the Pt MLX plot.

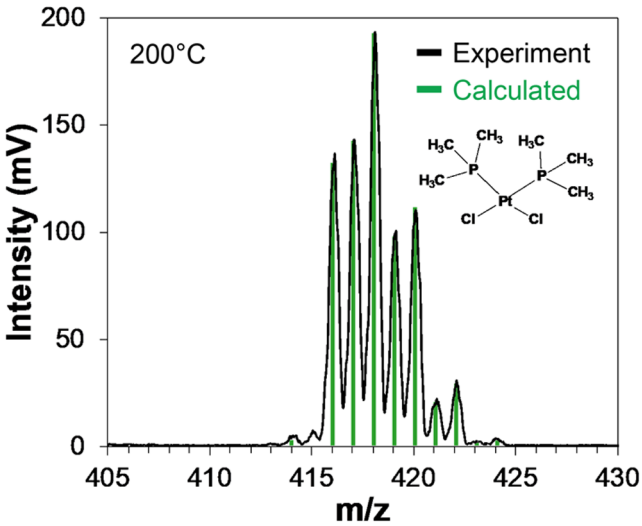

Figure 8. Mass spectrum of $PtCl_2(P(Me)_3)_2^+$ from $P(Me)_3$ exposure to $PtCl_2$ powder at 200 °C.

The intensity of the $PtCl_2(P(Me)_3)_2^+$ product as a function of the sample temperature is shown in Figure 9. For this linear temperature ramp experiment, the $PtCl_2(P(Me)_3)_2^+$ signals have an onset at 90 °C. This onset temperature is similar to the onset temperature for $PdCl_2(P(Me)_3)_2^+$ at 85 °C as shown in

https://doi.org/10.1021/acs.jpcc.1c10690
J. Phys. Chem. C 2022, 126, 8287−8295

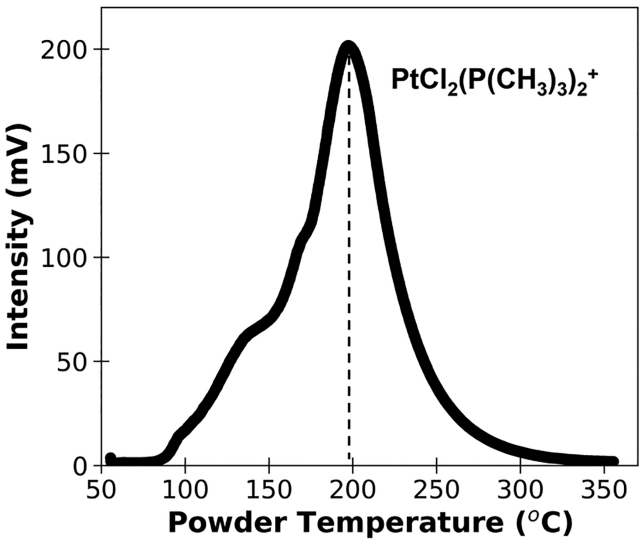

Figure 9. Ion intensity of $PtCl_2(P(Me)_3)_2^+$ as a function of powder temperature during $P(Me)_3$ exposure to $PtCl_2$ powder.

Figure 7. The peak ion intensity for $PtCl_2(P(Me)_3)_2^+$ is observed at 200 °C. This peak ion intensity is higher than the peak ion intensity observed at 150 °C for $PdCl_2(P(Me)_3)_2^+$ in Figure 7. Ion intensities for $PtCl_2(P(Me)_3)_2^+$ are observed at temperatures as high as 280 °C.

In addition to the MX_2L_2 complexes observed for Ni, Pd, and Pt, a new complex was also observed by exposing $P(Me)_3$ to $PtCl_2$ powder. This new complex has a stoichiometry of MX_4L_2. Figure 10a shows the ion intensities for this MX_4L_2 complex that was assigned to $PtCl_4(P(Me)_3)_2$. This assignment was confirmed by the characteristic Pt and Cl isotopic abundances. The experimental ion intensities and the calculated ion intensities based on the isotopic abundances are in excellent agreement as shown in Figure 10a.

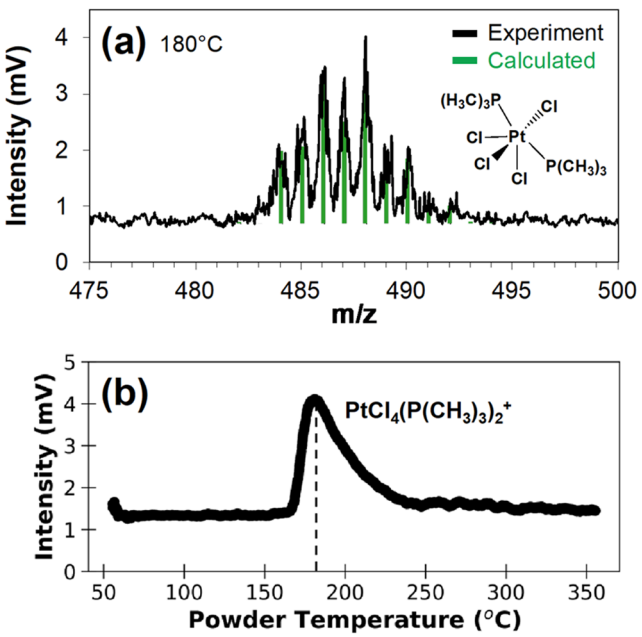

Figure 10. (a) Mass spectra of $PtCl_4(P(Me)_3)_2^+$ from $P(Me)_3$ exposure to $PtCl_2$ powder at 180 °C and (b) ion intensity of $PtCl_4(P(Me)_3)_2$ as a function of powder temperature during $P(Me)_3$ exposure to $PtCl_2$ powder.

The PtX_4L_2 complex has the second highest abundance probability of occurrence of 11% on the Pt MLX plot from the CBC method.[46] To the best of our knowledge, $PtCl_4(P(Me)_3)_2$ has not been reported in the literature. However, a close analogy to this complex is $PtCl_4(P(Et)_3)_2$ where Et = ethyl group, CH_2CH_3. The crystal structure of $PtCl_4(P(Et)_3)_2$ has been reported previously.[60] The possible chemical structure of $PtCl_4(P(Me)_3)_2$ is proposed in Figure 10a.

The intensity of the $PtCl_4(P(Me)_3)_2^+$ product as a function of the sample temperature is shown in Figure 10b. The $PtCl_4(P(Me)_3)_2^+$ signals have an onset at 165 °C. The peak ion intensity for $PtCl_2(P(Me)_3)_2^+$ is observed at 180 °C. This temperature for the peak ion intensity is higher than the temperature for the peak ion intensities of $NiCl_2(P(Me)_3)_2^+$ and $PdCl_2(P(Me)_3)_2^+$ and similar to $PtCl_2(P(Me)_3)_2^+$. Ion intensities for $PtCl_4(P(Me)_3)_2^+$ are observed at temperatures as high as 230 °C.

3.E. Computational Results of Ligand Addition of $P(Me)_3$ to MCl_2. Computational results for the ligand addition of $P(Me)_3$ to $NiCl_2$, $PdCl_2$ and $PtCl_2$ support the experimental observations. Calculations show that the addition of $P(Me)_3$ to the metal chlorides is thermodynamically favorable for both the first and second $P(Me)_3$ ligand-addition reactions. Figure 11 displays the changes in Gibbs free energy for the stepwise $P(Me)_3$ ligand addition to $NiCl_2$, $PdCl_2$, and $PtCl_2$ calculated at 100 °C.

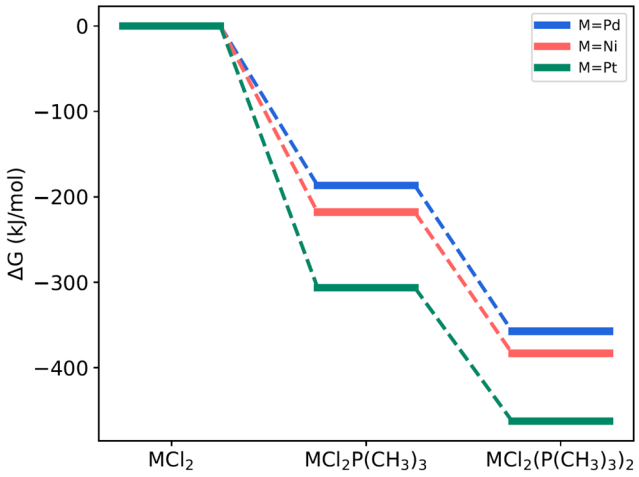

Figure 11. Thermochemistry of ligand addition of $P(Me)_3$ to MCl_2 and $MCl_2(P(Me)_3)$ where M = Ni, Pd, Pt. Change in Gibbs free energy is calculated at 100 °C.

The first ligand addition of $P(Me)_3$ is favorable as indicated by the negative change in free energy. The free energy change for the first ligand addition is largest for $PtCl_2$ at −306 kJ/mol. The free energy changes for the first ligand addition are −218 and −186 kJ/mol for $NiCl_2$ and $PdCl_2$, respectively. The total free energy change after the second ligand addition is largest for $PtCl_2$ at −463 kJ/mol. The total free energy changes after the second ligand addition are −383 and −357 kJ/mol for $NiCl_2$ and $PdCl_2$, respectively. These theoretical calculations support ligand addition of $P(Me)_3$ to MCl_2 as an effective pathway to produce stable $MCl_2(P(Me)_3)_2$ complexes.

3.F. Recent Results for Ni Thermal ALE and Predictions for Pd and Pt Thermal ALE. The identification

https://doi.org/10.1021/acs.jpcc.1c10690
J. Phys. Chem. C 2022, 126, 8287−8295

of volatile products from spontaneous etching of $NiCl_2$, $PdCl_2$, and $PtCl_2$ by ligand addition with $P(Me)_3$ are predictive for Ni, Pd, and Pt thermal ALE using chlorination and ligand-addition reactions. The $NiCl_2$, $PdCl_2$, and $PtCl_2$ metal chlorides represent Ni, Pd, and Pt after chlorination reactions. The QMS studies of the reaction of $P(Me)_3$ with $NiCl_2$, $PdCl_2$, and $PtCl_2$ powders model the ligand-addition reaction for volatile release. The observation of the $NiCl_2(P(Me)_3)_2$, $PdCl_2(P(Me)_3)_2$, and $PtCl_2(P(Me)_3)_2$ volatile etch products indicates that Ni, Pd, and Pt thermal ALE should be possible.

Recent studies of Ni thermal ALE have been reported using SO_2Cl_2 for chlorination and $P(Me)_3$ for ligand addition.[47] A number of experiments including quartz crystal microbalance (QCM) and X-ray reflectivity (XRR) measurements obtained Ni ALE etch rates versus temperature. The etch rates obtained from the QCM measurements were 0.14, 0.57, 0.67, 1.30, and 3.07 Å/cycle at 75, 100, 125, 150, and 175 °C, respectively. These results indicate that the observation of $NiCl_2(P(Me)_3)_2$ from $P(Me)_3$ exposures on $NiCl_2$ powders in the current study is consistent with the feasibility of Ni thermal ALE using SO_2Cl_2 and $P(Me)_3$ as the reactants.

The Ni ALE etch rates increased with temperature, and the largest Ni ALE etch rate of 3.07 Å/cycle was observed at the highest temperature of 175 °C.[47] In contrast, Figure 3 shows that the $NiCl_2(P(Me)_3)_2$ volatile etch products from $P(Me)_3$ exposures on $NiCl_2$ powders peaked at 92 °C during the temperature ramp and then decreased to a negligible QMS signal intensity at 175 °C. This contrast may be related to the different nature of the nickel chloride produced by SO_2Cl_2 chlorination of nickel and the $NiCl_2$ powder. The $NiCl_2$ powder is crystalline, whereas the thin nickel chloride layer on the Ni substrate after chlorination by SO_2Cl_2 during Ni thermal ALE may be more amorphous. These structural differences may lead to varying rates of ligand addition with $P(Me)_3$.

The good agreement between the observation of $NiCl_2(P(Me)_3)_2$ from $P(Me)_3$ exposures on $NiCl_2$ and the demonstration of Ni thermal ALE using SO_2Cl_2 and $P(Me)_3$ as the reactants can also lead to predictions for Pd and Pt thermal ALE. The detection of $PdCl_2(P(Me)_3)_2$ and $PtCl_2(P(Me)_3)_2$ from $P(Me)_3$ exposures on $PdCl_2$ and $PtCl_2$, respectively, suggests that Pd and Pt thermal ALE should be possible using SO_2Cl_2 and $P(Me)_3$ as the reactants. Additional thermal ALE experiments are needed to verify these predictions.

4. CONCLUSIONS

The group 10 metal chlorides, $NiCl_2$, $PdCl_2$, and $PtCl_2$, were spontaneously etched by ligand addition with $P(Me)_3$. Ligand addition of $P(Me)_3$ to these metal chlorides was able to form stable and volatile complexes. These ligand-addition reactions were suggested by the CBC method. The CBC method predicts that a complex with a stoichiometry of MX_2L_2 is most frequently observed for Ni, Pd, and Pt. Using chlorination and ligand addition with $P(Me)_3$ for these group 10 metals, the expected volatile product is $MCl_2(P(Me)_3)_2$.

In agreement with these expectations, *in situ* QMS studies revealed that $NiCl_2(P(Me)_3)_2^+$, $PdCl_2(P(Me)_3)_2^+$, and $PtCl_2(P(Me)_3)_2^+$ were observed as volatile metal complexes resulting from $P(Me)_3$ exposure to the group 10 metal chlorides. The assignment of these complexes was aided by the natural isotopic abundance of Ni, Pd, Pt, and Cl that led to distinct ion intensity fingerprints. Thermochemical calculations also confirmed that addition of $P(Me)_3$ to MCl_2 and $MCl_2(P(Me)_3)$ was favorable where M = Ni, Pd, and Pt.

The identification of the $MCl_2(P(Me)_3)_2$ volatile products suggests that Ni, Pd, and Pt can be etched by thermal atomic layer etching (ALE) methods. In agreement with this suggestion, results have been reported recently for thermal Ni ALE using SO_2Cl_2 for chlorination and $P(Me)_3$ for ligand addition. The etching of Pd, Pt, and other metals should be possible employing similar strategies using the CBC method for guidance on the necessary X and L ligands to form stable and volatile etch products.

■ AUTHOR INFORMATION

Corresponding Author

Steven M. George − *Department of Chemistry, University of Colorado, Boulder, Colorado 80309, United States;* orcid.org/0000-0003-0253-9184; Email: Steven.George@Colorado.edu

Authors

Ann Lii-Rosales − *Department of Chemistry, University of Colorado, Boulder, Colorado 80309, United States*

Virginia L. Johnson − *Department of Chemistry, University of Colorado, Boulder, Colorado 80309, United States*

Sandeep Sharma − *Department of Chemistry, University of Colorado, Boulder, Colorado 80309, United States*

Andreas Fischer − *Lam Research Corporation, Fremont, California 94538, United States*

Thorsten Lill − *Lam Research Corporation, Fremont, California 94538, United States*

Complete contact information is available at: https://pubs.acs.org/10.1021/acs.jpcc.1c10690

Notes

The authors declare no competing financial interest.

■ ACKNOWLEDGMENTS

This research was funded by Lam Research Corporation. The authors acknowledge Jessica Murdzek for useful discussions and motivating these studies by her results for Ni thermal ALE using sequential exposures of SO_2Cl_2 and PMe_3. Sandeep Sharma was partly supported by NSF Grant CHE-1800584.

■ REFERENCES

(1) Abe, H.; Yoneda, M.; Fujiwara, N. Developments of Plasma Etching Technology for Fabricating Semiconductor Devices. *Jpn. J. Appl. Phys.* **2008**, *47*, 1435−1455.

(2) Donnelly, V. M.; Kornblit, A. Plasma Etching: Yesterday, Today, and Tomorrow. *J. Vac. Sci. Technol. A* **2013**, *31*, 050825.

(3) Jansen, H.; Gardeniers, H.; de Boer, M.; Elwenspoek, M.; Fluitman, J. A Survey on the Reactive Ion Etching of Silicon in Microtechnology. *J. Micromech. Microeng.* **1996**, *6*, 14−28.

(4) Ibbotson, D. E.; Mucha, J. A.; Flamm, D. L.; Cook, J. M. Plasmaless Dry Etching of Silicon with Fluorine-Containing Compounds. *J. Appl. Phys.* **1984**, *56*, 2939−2942.

(5) Winters, H. F.; Coburn, J. W. Etching of Silicon with XeF_2 Vapor. *Appl. Phys. Lett.* **1979**, *34*, 70−73.

(6) Winters, H. F. The Etching of W(111) with XeF_2. *J. Vac. Sci. Technol. A* **1985**, *3*, 700−704.

(7) Winters, H. F. The Etching of Cu(100) with Cl_2. *J. Vac. Sci. Technol. A* **1985**, *3*, 786−790.

(8) Winters, H. F. Etch Products from the Reaction on Cl_2 with Al(100) and Cu(100) and XeF_2 with W(111) and Nb. *J. Vac. Sci. Technol. B* **1985**, *3*, 9−15.

(9) Fischer, A.; Routzahn, A.; George, S. M.; Lill, T. Thermal Atomic Layer Etching: A Review. *J. Vac. Sci. Technol. A* **2021**, *39*, 030801.
(10) George, S. M. Mechanisms of Thermal Atomic Layer Etching. *Acc. Chem. Res.* **2020**, *53*, 1151−1160.
(11) Mullins, R.; Natarajan, S. K.; Elliott, S. D.; Nolan, M. Self-Limiting Temperature Window for Thermal Atomic Layer Etching of HfO_2 and ZrO_2 Based on the Atomic-Scale Mechanism. *Chem. Mater.* **2020**, *32*, 3414−3426.
(12) Natarajan, S. K.; Cano, A. M.; Partridge, J. L.; George, S. M.; Elliott, S. D. Prediction and Validation of the Process Window for Atomic Layer Etching: HF Exposure on TiO_2. *J. Phys. Chem. C* **2021**, *125*, 25589−25599.
(13) Cano, A. M.; Natarajan, S. K.; Partridge, J. L.; Elliott, S. D.; George, S. M. Spontaneous Etching of B_2O_3 by HF Gas Studied Using Infrared Spectroscopy, Mass Spectrometry, and Density Functional Theory. *J. Vac. Sci. Technol. A* **2022**, *40*, 022601.
(14) Cano, A. M.; Marquardt, A. E.; DuMont, J. W.; George, S. M. Effect of HF Pressure on Thermal Al_2O_3 Atomic Layer Etch Rates and Al_2O_3 Fluorination. *J. Phys. Chem. C* **2019**, *123*, 10346−10355.
(15) Lee, Y.; DuMont, J. W.; George, S. M. Trimethylaluminum as the Metal Precursor for the Atomic Layer Etching of Al_2O_3 Using Sequential, Self-Limiting Thermal Reactions. *Chem. Mater.* **2016**, *28*, 2994−3003.
(16) Lee, Y.; George, S. M. Atomic Layer Etching of Al_2O_3 Using Sequential, Self-Limiting Thermal Reactions with $Sn(acac)_2$ and Hydrogen Fluoride. *ACS Nano* **2015**, *9*, 2061−2070.
(17) Lee, Y.; George, S. M. Thermal Atomic Layer Etching of HfO_2 Using HF for Fluorination and $TiCl_4$ for Ligand-Exchange. *J. Vac. Sci. Technol. A* **2018**, *36*, 061504.
(18) Lee, Y.; George, S. M. Thermal Atomic Layer Etching of Al_2O_3, HfO_2, and ZrO_2 Using Sequential Hydrogen Fluoride and Dimethylaluminum Chloride Exposures. *J. Phys. Chem. C* **2019**, *123*, 18455−18466.
(19) Zywotko, D. R.; George, S. M. Thermal Atomic Layer Etching of ZnO by a "Conversion-Etch" Mechanism Using Sequential Exposures of Hydrogen Fluoride and Trimethylaluminum. *Chem. Mater.* **2017**, *29*, 1183−1191.
(20) Lee, Y.; Johnson, N. R.; George, S. M. Thermal Atomic Layer Etching of Gallium Oxide Using Sequential Exposures of HF and Various Metal Precursors. *Chem. Mater.* **2020**, *32*, 5937−5948.
(21) Johnson, N. R.; Sun, H. X.; Sharma, K.; George, S. M. Thermal Atomic Layer Etching of Crystalline Aluminum Nitride Using Sequential, Self-limiting Hydrogen Fluoride and $Sn(acac)_2$ Reactions and Enhancement by H_2 and Ar Plasmas. *J. Vac. Sci. Technol. A* **2016**, *34*, 050603.
(22) Lee, Y.; George, S. M. Thermal Atomic Layer Etching of Titanium Nitride Using Sequential, Self-Limiting Reactions: Oxidation to TiO_2 and Fluorination to Volatile TiF_4. *Chem. Mater.* **2017**, *29*, 8202−8210.
(23) Johnson, N. R.; Hite, J. K.; Mastro, M. A.; Eddy, C. R.; George, S. M. Thermal Atomic Layer Etching of Crystalline GaN Using Sequential Exposures of XeF_2 and BCl_3. *Appl. Phys. Lett.* **2019**, *114*, 243103.
(24) Abdulagatov, A. I.; George, S. M. Thermal Atomic Layer Etching of Silicon Using O_2, HF, and $Al(CH_3)_3$ as the Reactants. *Chem. Mater.* **2018**, *30*, 8465−8475.
(25) DuMont, J. W.; Marquardt, A. E.; Cano, A. M.; George, S. M. Thermal Atomic Layer Etching of SiO_2 by a "Conversion-Etch" Mechanism Using Sequential Reactions of Trimethylaluminum and Hydrogen Fluoride. *ACS Appl. Mater. Interfaces* **2017**, *9*, 10296−10307.
(26) Abdulagatov, A. I.; George, S. M. Thermal Atomic Layer Etching of Silicon Nitride Using an Oxidation and "Conversion Etch" Mechanism. *J. Vac. Sci. Technol. A* **2020**, *38*, 022607.
(27) Abdulagatov, A. I.; Sharma, V.; Murdzek, J. A.; Cavanagh, A. S.; George, S. M. Thermal Atomic Layer Etching of Germanium-Rich SiGe Using an Oxidation and "Conversion-Etch" Mechanism. *J. Vac. Sci. Technol. A* **2021**, *39*, 022602.
(28) Johnson, N. R.; George, S. M. WO_3 and W Thermal Atomic Layer Etching Using "Conversion-Fluorination" and "Oxidation-Conversion-Fluorination" Mechanisms. *ACS Appl. Mater. Interfaces* **2017**, *9*, 34435−34447.
(29) Mohimi, E.; Chu, X. Q. I.; Trinh, B. B.; Babar, S.; Girolami, G. S.; Abelson, J. R. Thermal Atomic Layer Etching of Copper by Sequential Steps Involving Oxidation and Exposure to Hexafluoroacetylacetone. *ECS J. Solid State Sci. Technol.* **2018**, *7*, P491−P495.
(30) Konh, M.; He, C.; Lin, X.; Guo, X. Y.; Pallem, V.; Opila, R. L.; Teplyakov, A. V.; Wang, Z. J.; Yuan, B. Molecular Mechanisms of Atomic Layer Etching of Cobalt with Sequential Exposure to Molecular Chlorine and Diketones. *J. Vac. Sci. Technol. A* **2019**, *37*, 021004.
(31) George, S. M.; Lee, Y. Prospects for Thermal Atomic Layer Etching Using Sequential, Self-Limiting Fluorination and Ligand-Exchange Reactions. *ACS Nano* **2016**, *10*, 4889−4894.
(32) Osakada, K. Transmetalation. In *Current Methods in Inorganic Chemistry*; Kurosawa, H., Yamamoto, A., Eds.; Elsevier, 2003; Vol. 3, Chapter 5, pp 233−291.
(33) Lee, Y.; Huffman, C.; George, S. M. Selectivity in Thermal Atomic Layer Etching Using Sequential, Self-Limiting Fluorination and Ligand-Exchange Reactions. *Chem. Mater.* **2016**, *28*, 7657−7665.
(34) Lii-Rosales, A.; Cavanagh, A. S.; Fischer, A.; Lill, T.; George, S. M. Spontaneous Etching of Metal Fluorides Using Ligand-Exchange Reactions: Landscape Revealed by Mass Spectrometry. *Chem. Mater.* **2021**, *33*, 7719−7730.
(35) Fischer, A.; Routzahn, A.; Lee, Y.; Lill, T.; George, S. M. Thermal Etching of AlF_3 and Thermal Atomic Layer Etching of Al_2O_3. *J. Vac. Sci. Technol. A* **2020**, *38*, 022603.
(36) Crabtree, R. H. *The Organometallic Chemistry of the Transistion Metals*, 6th ed.; John Wiley & Sons, Inc.: Hoboken, NJ, 2014.
(37) Daul, C.; Emmenegger, F.; Mlinar, M.; Piccand, M. Gaseous Complexes of $CoCl_2$ with Pyridine. *Inorg. Chem.* **1993**, *32*, 2992−2995.
(38) Emmenegger, F. Volatile Metal-Complexes. *Chimia* **1994**, *48*, 341−342.
(39) Farkas, J.; Chi, K. M.; Hampden-Smith, M. J.; Kodas, T. T.; Dubois, L. H. Etching of Copper and Copper-Oxide at High Rates via Generation of Volatile Copper Species. *Mater. Sci. Eng., B* **1993**, *17*, 93−96.
(40) Farkas, J.; Chi, K. M.; Hampden-Smith, M. J.; Kodas, T. T.; Dubois, L. H. Low-Temperature Copper Etching via Reactions with Cl_2 and PEt_3 Under Ultrahigh Vacuum Conditions. *J. Appl. Phys.* **1993**, *73*, 1455−1460.
(41) Hampden-Smith, M. J.; Kodas, T. T. Copper Etching: New Chemical Approaches. *MRS Bull.* **1993**, *18*, 39−45.
(42) Mameli, A.; Verheijen, M. A.; Mackus, A. J. M.; Kessels, W. M. M.; Roozeboom, F. Isotropic Atomic Layer Etching of ZnO Using Acetylacetone and O_2 Plasma. *ACS Appl. Mater. Interfaces* **2018**, *10*, 38588−38595.
(43) Lin, X.; Chen, M. X.; Janotti, A.; Opila, R. In situ XPS Study on Atomic Layer Etching of Fe Thin Film Using Cl_2 and Acetylacetone. *J. Vac. Sci. Technol. A* **2018**, *36*, 051401.
(44) Green, M. L. H. A New Approach to the Formal Classification of Covalent Compounds of the Elements. *J. Organomet. Chem.* **1995**, *500*, 127−148.
(45) *Dictionary of Organometallic Compounds*, 2nd ed.; Chapman & Hall Scientific Data Division: London, 1995.
(46) The Covalent Bond Classification Method: A New Approach to the Formal Classification of Covalent Compounds of the Elements. http://www.columbia.edu/cu/chemistry/groups/parkin/cbc.htm (accessed March 2022).
(47) Murdzek, J. A.; Lii-Rosales, A.; George, S. M. Thermal Atomic Layer Etching of Nickel Using Sequential Chlorination and Ligand-Addition Reactions. *Chem. Mater.* **2021**, *33*, 9174−9183.
(48) Hutzler, N. R.; Lu, H. I.; Doyle, J. M. The Buffer Gas Beam: An Intense, Cold, and Slow Source for Atoms and Molecules. *Chem. Rev.* **2012**, *112*, 4803−4827.

https://doi.org/10.1021/acs.jpcc.1c10690
J. Phys. Chem. C 2022, 126, 8287−8295

(49) Frisch, M. J.; Trucks, G. W.; Schlegel, H. B.; Scuseria, G. E.; Robb, M. A.; Cheeseman, J. R.; Scalmani, G.; Barone, V.; Petersson, G. A.; Nakatsuji, H.; et al. *Gaussian 16*, revision C.01; Gaussian Inc.: Wallingford, CT, 2016.
(50) Lee, C.; Yang, W.; Parr, R. G. Development of the Colle-Salvetti Correlation-Energy Formula Into a Functional of the Electron Density. *Phys. Rev. B* **1988**, *37*, 785−789.
(51) Weigend, F.; Ahlrichs, R. Balanced Basis Sets of Split Valence, Triple Zeta Valence and Quadruple Zeta Valence Quality for H to Rn: Design and Assessment of Accuracy. *Phys. Chem. Chem. Phys.* **2005**, *7*, 3297−3305.
(52) Purvis, G. D., III; Bartlett, R. J. A Full Coupled-Cluster Singles and Doubles Model: The Inclusion of Disconnected Triples. *J. Chem. Phys.* **1982**, *76*, 1910−1918.
(53) Scuseria, G. E.; Janssen, C. L.; Schaefer, H. F., III An Efficient Reformulation of the Closed-Shell Coupled Cluster Single and Double Excitation (CCSD) Equations. *J. Chem. Phys.* **1988**, *89*, 7382−7387.
(54) Scuseria, G. E.; Schaefer, H. F., III Is Coupled Cluster Singles and Doubles (CCSD) More Computationally Intensive than Quadratic Configuration Interaction (QCISD)? *J. Chem. Phys.* **1989**, *90*, 3700−3703.
(55) Dunning, T. H., Jr.; Hay, P. J. *Modern Theoretical Chemistry*; Plenum: New York, 1977.
(56) Dill, K. A.; Bromberg, S. *Molecular Driving Forces: Statistical Thermodynamics in Biology, Chemistry, Physics and Nanoscience*, 2nd ed.; Garland Science: New York, NY, 2011.
(57) Anderson, J.; Burns, P. J.; Milroy, D.; Ruprecht, P.; Hauser, T.; Siegel, H. J. Deploying RMACC Summit: An HPC Resource for the Rocky Mountain Region. *Proceedings of PEARC 17*; ACM, 2017; p 7.
(58) King, D. A.; Wells, M. G. Reaction Mechanism in Chemisorption Kinetics: Nitrogen on (100) Plane of Tungsten. *Proc. R. Soc. London, Ser. A* **1974**, *339*, 245−269.
(59) Lam, H. W. Bis(trimethylphosphine)nickel Dichloride. In *Encyclopedia of Reagents for Organic Synthesis*; Wiley, 2011.
(60) Hitchcock, P. B.; Jacobson, B.; Pidcock, A. Bond Lengths in Platinum(II) and Platinum(IV) Complexes. Crystal and Molecular Structure of cis-tetrachlorobis(triethylphosphine) platinum(IV). *J. Organomet. Chem.* **1977**, *136*, 397−405.

https://doi.org/10.1021/acs.jpcc.1c10690
J. Phys. Chem. C 2022, 126, 8287−8295